Box atlas: An interval version of atlas

Arthur Ignazi, Rémy Guyonneau, Sébastien Lagrange, Sébastien Lahaye

Box Atlas: an Interval Version of Atlas

Arthur Ignazi[a], Remy Guyonneau[a], Sébastien Lagrange[a], Sébastien Lahaye[a]

[a] *Univ Angers, LARIS, SFR MATHSTIC, F-49000, Angers, France*

Abstract

This paper presents an adaptation of the notion of atlas to interval analysis named box atlas. This new concept makes it possible to directly use interval analysis methods on compact manifolds. This can be useful to solve path planning problems or to compute attainability in robotics. To demonstrate the relevance of the approach, a box atlas for two classic manifolds is proposed and an application for a path planning problem is presented. The paper also proposes a paving construction for every compact manifolds of dimension 2 that is box atlas compatible.

Keywords: Manifolds, Atlas, Interval analysis, Path planning

1. Introduction

Among the various ways to describe manifolds, atlases are one of the most common tools [1]. In topology, an atlas serves as a collection of charts that provide coordinates on the manifold. These charts describe homeomorphisms, or smooth mappings, between subsets of the manifold and subsets of Euclidean spaces like $\mathbb{R}^n$. By using charts, one can perform computations locally, in Euclidean spaces, rather than directly on the manifold.

On a different but related note, interval analysis [2, 3] plays a significant role in robotics, particularly in applications such as path planning [4] and localization [5, 6]. What makes interval analysis particularly appealing in these contexts is its ability to account for rounding errors, ensuring that solutions are robust and reliable. Numerous methods within interval analysis can be applied to these problems, making it a versatile tool in robotics [7, 8].

In this context, the paper introduces a novel approach named **box atlas** for describing manifolds that permits to use interval analysis methods. It offers a description of manifolds that seamlessly integrates with interval-based

tools. The core idea is to construct atlas-like descriptions where each chart is directly compatible with interval analysis. While applying interval methods to a manifold itself can be challenging, working with charts allows interval tools to be used more effectively, with results that can later be translated back to the manifold. A method named "bisectable abstract domain" [9] makes it possible to treat manifolds using interval analysis on manifolds where a lattice structure (with inclusion) can be defined. The box atlas presented in this paper is an alternative to "bisectable abstract domain" that makes it possible to bisect domains and define an intersection on sets that are not lattices. For instance, the box atlas allows using interval analysis on non-orientable manifolds (such as projective plane or Klein bottle).

In robotics, the importance of accurately modeling a robot's configuration space cannot be overstated, especially when it comes to path planning and other motion-related tasks. As highlighted in [10], manifolds are used in almost all robotics applications, even when they are not modeled explicitly. The configuration space of a robot, which represents all possible positions and orientations of the robot, is typically described by a mathematical structure known as a manifold [11, 12, 13]. By understanding this space, algorithms that help robots navigate and perform tasks efficiently can be designed. That is why box atlas can be applied in robotics.

The paper is structured as follows: Section 2 covers the necessary mathematical background on manifolds and interval analysis. Section 3 introduces the box atlas approach. Section 4 proposes a path planning application of the proposed method. Finally, Section 5 provides a summary and discusses potential future directions for this research.

2. Mathematical background

The mathematical background required to understand the concept introduced in this paper is presented in this section.

2.1. Manifold

Manifolds [14] makes it possible to represent complex, high-dimensional spaces in a structured way. They are used in numerous subjects such as robotics [15], machine learning [16], geometry [17]. This subsection covers the basics of manifolds, with a focus on the main representation of manifolds, that are atlases.

A manifold is a space that, while potentially complex globally, resembles Euclidean space locally. There exists a lot of categories of manifolds: manifolds with boundaries, differentiable manifolds, Lie group, Riemannian manifolds... In this paper, a specific family of manifolds is considered: the compact manifolds. A compact manifold is a manifold that can be covered by a finite number of open sets. This is the case for example of a circle, a torus, a Klein bottle.

To represent manifolds, one can use the external view. That is, representing the manifold in a space using more coordinates. For instance, the circle (dimension 1) can be embedded in $\mathbb{R}^2$, the sphere (dimension 2) can be embedded in $\mathbb{R}^3$, and the Klein bottle (dimension 2) can be embedded in $\mathbb{R}^4$.

Another representation, the one considered in this paper, is the internal view, called atlases. It relies on decomposing the manifold into multiple charts to constitute an atlas.

Definition 1. An atlas of a manifold M is an indexed family $\{(U_i, \varphi_i) : i \in I\}$ of charts $V_i = \varphi_i(U_i)$ such that $\bigcup_{i \in I} U_i = M$ where $U_i \subset M$ is an open set, φ_i is an homeomorphism and I is the number of charts.

Remark. I is not required to be finite, but in practice it is often finite or locally finite.

There exists a *transition map* τ_{ij} between each pair of charts V_i and V_j, defined on their intersection:

$$\forall x \in V_i, \tau_{ij}(x) = \varphi_j(\varphi_i^{-1}(x)). \tag{1}$$

If $U_i \cap U_j = \emptyset$, then $\forall x \in V_i, \tau_{ij}(x) = \emptyset$.

Decomposing a manifold into charts makes it possible to work either on euclidean space or simpler topological structures.

Many atlases can be constructed for a given manifold, depending on the number of charts chosen or the homeomorphisms built.

2.2. Interval analysis

This subsection presents the notions related to interval analysis. A bounded closed real interval $[x] = [\underline{x}, \overline{x}]$ is a set which can be written as $\{x \in \mathbb{R} : \underline{x} \leq x \leq \overline{x}\}$ with $\underline{x}$ and $\overline{x}$ in $\mathbb{R}$. The set of bounded closed real intervals is usually denoted by $\mathbb{IR}$. Interval analysis extends arithmetic

operators and functions such as addition, multiplication, cosine, exponential... Intervals are closed sets of dimension 1, whereas boxes (or interval vectors) $[\mathbf{x}] = [x_1] \times [x_2] \times \cdots \times [x_n]$ of $\mathbb{R}^n$ are the cartesian product of n intervals. The set of boxes is usually denoted $\mathbb{IR}^n$. The dimension of a box $\mathbf{x} \subset \mathbb{IR}^n$ is the number of intervals that compose it: $dim(\mathbf{x}) = n$. Most operators and functions applicable on intervals are applicable on boxes.

As mentioned in the previous paragraph, interval analysis extends classical functions like cosine or exponential. This is possible using inclusion functions. An inclusion function $[f]$ of a function f is a function that envelops the direct image of a box $[\mathbf{x}]$ by f:

$$\forall [\mathbf{x}] \in \mathbb{IR}^n, f([\mathbf{x}]) \subset [f]([\mathbf{x}]).$$

An example of an inclusion function is depicted in Figure 1.

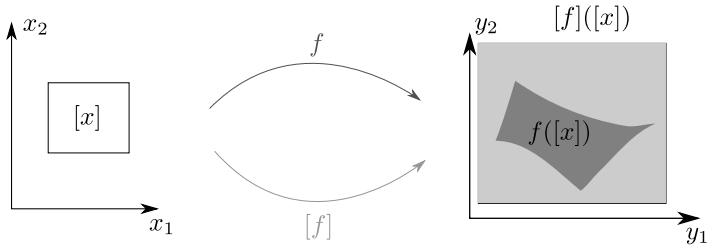

Figure 1: An inclusion function of f.

In addition to the classic set functions, new methods have been introduced using interval analysis. One of the most known and used is SIVIA (Set Inversion Via Interval Analysis) [18]. It is a subdivision algorithm that solves a set inversion problem using interval analysis.

A set inversion problem is a technique used to characterize the antecedent $\mathbb{X}$ of a function f based on its image $\mathbb{Y}$:

$$\mathbb{X} = \{x \in \mathbb{R}^n | f(x) \in \mathbb{Y}\} = f^{-1}(\mathbb{Y}).$$

SIVIA algorithm approximates $\mathbb{X}$ by two subpavings $\mathbb{X}^-$ and $\mathbb{X}^+$ such that $\mathbb{X}^- \subset \mathbb{X} \subset \mathbb{X}^+$.

To test if a box $[\mathbf{x}]$ is in the solution $\mathbb{X}$, the following tests are used:

$$\begin{array}{lllll} \text{(i)} & [f]([\mathbf{x}]) \subset \mathbb{Y} & \Rightarrow & [\mathbf{x}] \subset \mathbb{X}; \\ \text{(ii)} & [f]([\mathbf{x}]) \cap \mathbb{Y} = \emptyset & \Rightarrow & [\mathbf{x}] \cap \mathbb{X} = \emptyset. \end{array}$$

If both tests failed, $[\mathbf{x}]$ is bisected until it is smaller than a fixed accuracy ε. A box is bisected when it is split in two equal parts separated by its principal plan. The subpaving $\mathbb{X}^-$ contains all the boxes satisfying the first test. The subpaving $\mathbb{X}^+$ contains $\mathbb{X}^-$ and all the boxes for which all the interval components are smaller than ε.

3. Box Atlas

On the first hand, most configuration spaces in robotics can be represented as manifolds. On the other hand, interval analysis implements a lot of methods on robotic examples, but the configuration space of the robots must be boxes. The idea behind the box atlas (the original contribution presented in this paper) is to create a subclass of atlases for which it is possible to apply interval analysis methods on the charts.

Definition 2. A box atlas of a compact manifold M is an indexed family $\{(U_i, \varphi_i) : i \in I\}$, with I finite, of charts $V_i = \varphi_i(U_i)$ such that

- U_i are closed subsets of M
- $\forall i, j \in I, (i \neq j) : dim(U_i \cap U_j) < dim(U_i)$
- $\bigcup_{i \in I} U_i = M$
- the charts V_i are boxes
- φ_i are the homeomorphisms such that $V_i = \varphi_i(U_i)$.

Some properties differ from the classical atlas definition. The charts V_i are boxes to be able to apply interval analysis in the charts. As φ_i are homeomorphisms between U_i and V_i, U_i are closed sets. To avoid redundancy when subdivision algorithms such as SIVIA are applied on charts, the intersection between two charts is defined to have a lower dimension than the involved charts.

Remark. As for the atlas, there exists a transition map τ_{ij} between each pair of charts (V_i, V_j). If $U_i \cap U_j = \emptyset$, then $\forall x \in V_i, \tau_{ij}(x) = \emptyset$.

Box atlas can be used to describe compact manifolds by decomposing it into multiples charts that are boxes. Interval analysis methods such as SIVIA can be applied on each chart, and a global result can be observed

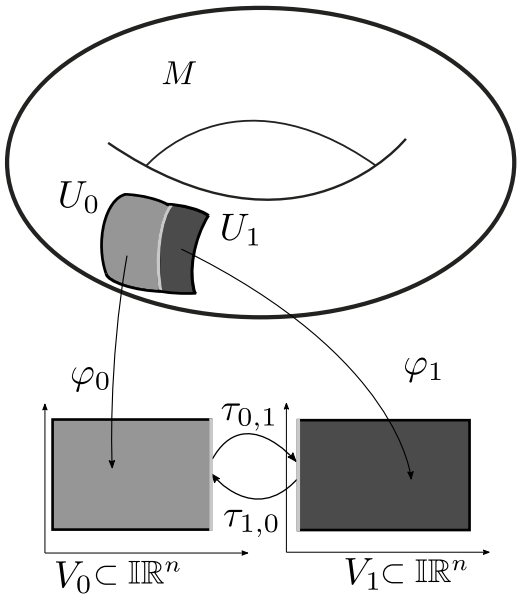

Figure 2: Two charts of a box atlas of M.

using transition maps. Figure 2 presents two charts of a box atlas and their transition maps.

Box atlas can be built separately or by using existing box atlases. The following proposition allows to obtain a box atlas of a compact manifold resulting of the cartesian product of two compact manifolds which have their own box atlas. This proposition is an extension of a property of atlases.

Proposition 1. The box atlas being a subclass of atlases, if $\{U_i, \varphi_i\}$ is a box atlas of M of dimension m and $\{W_j, \psi_j\}$ is a box atlas of N of dimension n, then $\{U_i \times W_j, \varphi_i \times \psi_j : U_i \times W_j \to \mathbb{R}^m \times \mathbb{R}^n\}$ is a box atlas of $M \times N$.

Proof. Let M be a manifold and N be a manifold. $\{U_i, \varphi_i\}$ is an atlas of M and $\{W_j, \psi_j\}$ is an atlas of N. Proof 5.18 of [14] specifies that $\{U_i \times W_j, \varphi_i \times \psi_j : U_i \times W_j \to \mathbb{R}^m \times \mathbb{R}^n\}$ is an atlas of $M \times N$ and $M \times N$ is a manifold of dimension $m + n$. The atlas inducted is a box atlas, according to Definition 2. □

The sections 3.1 and 3.2 present two examples of box atlases with interval analysis methods applied on them. Section 3.3 presents an iterative method to make a box atlas-compatible paving of the surfaces, according to Definition 2.

φ_0:	φ_1:
$U_0 \rightarrow V_0$	$U_1 \rightarrow V_1$
$(\alpha) \mapsto (\alpha/\pi)$	$(\alpha) \mapsto ((\alpha-\pi)/\pi)$
φ_0^{-1}:	φ_1^{-1}:
$V_0 \rightarrow U_0$	$V_1 \rightarrow U_1$
$(x_0) \mapsto (x_0 \cdot \pi)$	$(x_1) \mapsto ((x_1+1) \cdot \pi)$

Table 1: Homeomorphisms for the box atlas of the circle.

Note that in the continuation of this paper, an interval $[\underline{x}, \overline{x}]$ in the chart V_i will be noted $[\underline{x}, \overline{x}]_{V_i}$.

3.1. Box atlas of the circle

3.1.1. Construction

This subsection presents a box atlas for the compact manifold S^1. In topology, the circle S^1 is defined by $[0, 2\pi]$ where $0 \sim 2\pi$. It can be split in two subsets: $U_0 = [0, \pi]$ and $U_1 = [\pi, 2\pi]$. The union of those subsets covers the circle.

V_0 and V_1 can be chosen arbitrarily in $\mathbb{R}^1$. Let's define the charts $V_0 = [0, 1]$ and $V_1 = [0, 1]$. Homeomorphisms φ_0 and φ_1 can be defined to give transformations from the manifold to the two charts as stated in Table 1.

Figure 3 illustrates the box atlas of the circle.

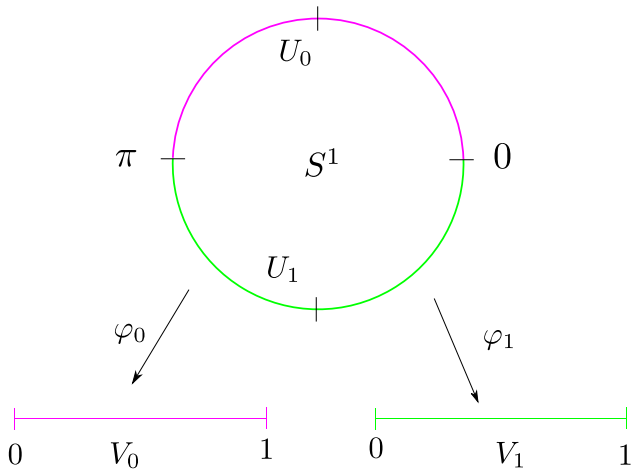

Figure 3: A box atlas of the circle.

V_0 and V_1 are of dimension 1. There exist transition maps between V_0 and V_1. These transition maps $\tau_{0,1}$ and $\tau_{0,1}$ are defined by:

$$\tau_{0,1}(x_0) = \begin{cases} 0 & \text{for } x_0 = 1 \\ 1 & \text{for } x_0 = 0 \\ \emptyset & \text{otherwise} \end{cases}$$

$$\tau_{1,0}(x_1) = \begin{cases} 0 & \text{for } x_1 = 1 \\ 1 & \text{for } x_1 = 0 \\ \emptyset & \text{otherwise} \end{cases}$$

The intersections between the subsets U_0 and U_1 of the manifold are of dimension 0. The transition map shows that the two charts are linked by only two points.

Remark. Since the charts V_i are boxes, the function φ_i are homeomorphisms and the subsets of the manifold U_i are closed sets, a box atlas of the circle has at least two charts. Indeed, a box atlas of the circle S^1 with a single chart would be the closed subset $U_0 = [0, 2\pi]$, the homeomorphism $\varphi_0(x) = x/2\pi$ and the chart $V_0 = [0, 1]$. In this case, according to the topology of the circle ($0 \sim 2\pi$), so $\varphi_0(0) = 0$ and $\varphi_0(0) = \varphi_0(2\pi) = 1$ then φ_0 is not an homeomorphism. Thus, this is not a box atlas.

3.1.2. Use case

To illustrate the interest of such a box atlas, let's consider the following problem of angle calculation. Angles are periodic, with values repeating every 2π radians. That is, interval like $[7\pi/4, \pi/4]$ might seem invalid under standard interval notation, but it actually represents a continuous range due to the periodic nature of angles. It is preferred the notation $[7\pi/4, 9\pi/4]$. For each operation, intervals of angle should be normalized that make calculus tedious work. For instance, the intersection of $[\alpha] = [0, 9\pi/8]$ and $[\beta] = [7\pi/8, 18\pi/8]$ results to only one interval $[\alpha] \cap [\beta] = [7\pi/8, 9\pi/8]$. But assuming that $[\alpha]$ and $[\beta]$ are angles, it exists another intersection near 0 as it can be seen in Figure 4. This is due to the periodicity of angles, $[\alpha] = [0, 9\pi/8] = [2\pi, 25\pi/8]$. Then, $[\alpha] \cap [\beta] = [7\pi/8, 9\pi/8] \sqcup [2\pi, 18\pi/8]$. Normalized, the intersection is equal to $[0, 2\pi/8] \sqcup [7\pi/8, 9\pi/8]$. Figure 4 represents the angles on the circle.

Now let's use the box atlas of the circle defined in subsection 3.1.1. α and β belong to the manifold S^1 where the two charts V_0 and V_1 are depicted

in Figure 4. The homeomorphisms φ_0 and φ_1 are expressed in Table 1. $\varphi_0(\alpha) = [0, 1]$ and $\varphi_0(\beta) = [0, 2/8] \sqcup [7/8, 1]$. In V_0, $\alpha \cap \beta = [0, 2/8] \sqcup [7/8, 1]$. $\varphi_1(\alpha) = [0, 1/8]$ and $\varphi_1(\beta) = [0, 1]$ and in V_1, $\alpha \cap \beta = [0, 1/8]$. Then $\alpha \cap \beta = [0, 2/8]_{V_0} \sqcup [7/8, 1]_{V_0} \sqcup [0, 1/8]_{V_1}$. Using φ_0^{-1} and φ_1^{-1}, it gives $\alpha \cap \beta = [0, 2\pi/8] \sqcup [7\pi/8, 9\pi/8]$. The intersection of angles with interval analysis has been made easier using box atlas.

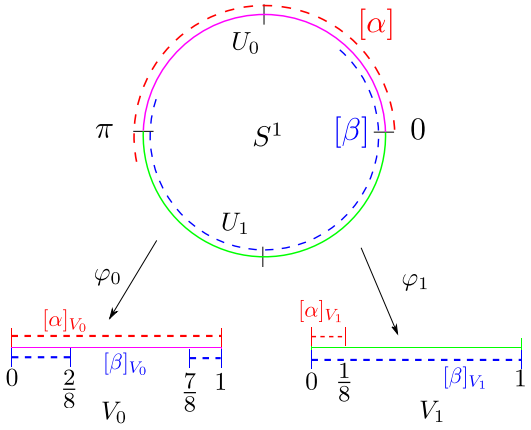

Figure 4: α and β on the circle and on each chart of the box atlas of S^1.

3.2. Box atlas of the torus

3.2.1. Construction

The second example is a box atlas of the torus $T^2 = S^1 \times S^1$, which is a compact manifold. According to Proposition 1, the box atlas of the torus can be constructed using the product of two box atlases of the circle.

The torus can be decomposed in 4 subsets: $U_0 = [0, \pi] \times [0, \pi]$, $U_1 = [\pi, 2\pi] \times [0, \pi]$, $U_2 = [0, \pi] \times [\pi, 2\pi]$, $U_3 = [\pi, 2\pi] \times [\pi, 2\pi]$.

As for the circle, the V_i can be chosen arbitrarily in $\mathbb{R}^2$. Let's define the charts $V_0 = V_1 = V_2 = V_3 = [0, 1] \times [0, 1]$. Homeomorphisms φ_i give transformations from the manifold to the charts as stated in Table 2.

Figure 5 illustrates this torus box atlas.

φ_0: $U_0 \rightarrow V_0$ $(\alpha, \beta) \mapsto (\alpha/\pi, \beta/\pi)$ φ_0^{-1}: $V_0 \rightarrow U_0$ $(x_0, y_0) \mapsto (x_0 \cdot \pi, y_0 \cdot \pi)$	φ_1: $U_1 \rightarrow V_1$ $(\alpha, \beta) \mapsto ((\alpha - \pi)/\pi, \beta/\pi)$ φ_1^{-1}: $V_1 \rightarrow U_1$ $(x_1, y_1) \mapsto ((x_1 + 1) \cdot \pi, y_1 \cdot \pi)$
φ_2: $U_2 \rightarrow V_2$ $(\alpha, \beta) \mapsto (\alpha/\pi, (\beta - \pi)/\pi)$ φ_2^{-1}: $V_2 \rightarrow U_2$ $(x_2, y_2) \mapsto (x_2 \cdot \pi, (y_2 + 1) \cdot \pi)$	φ_3: $U_3 \rightarrow V_3$ $(\alpha, \beta) \mapsto ((\alpha - \pi)/\pi, (\beta - \pi)/\pi)$ φ_3^{-1}: $V_3 \rightarrow U_3$ $(x_3, y_3) \mapsto ((x_3 + 1) \cdot \pi, (y_3 + 1) \cdot \pi)$

Table 2: Homeomorphisms for the box atlas of the torus.

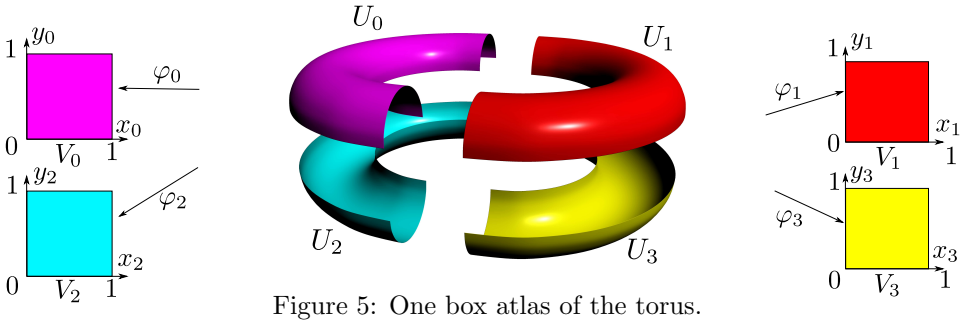

Figure 5: One box atlas of the torus.

3.2.2. Use case

In robotics, the $2R$ robot, a two arms robot with two elbows, is a well-known example. The configuration space of the robot is the cartesian product of the two angles $\alpha \in S^1$ and $\beta \in S^1$, i.e. a torus.

Figure 6 depicts this robot with an obstacle in its working space.

The geometric model of the robot [19] is given by:

$$\begin{pmatrix} x_B \\ y_B \end{pmatrix} = \begin{pmatrix} l_1 \cos(\alpha) + l_2 \cos(\alpha - \beta) \\ l_1 \sin(\alpha) + l_2 \sin(\alpha - \beta) \end{pmatrix}. \tag{2}$$

As the obstacle is constraining the robot, the set of allowed configurations $\mathbb{X} \subset T^2$ can be searched, that is where coordinates (x_A, y_A) and coordinates (x_B, y_B), do not intersect the obstacle.

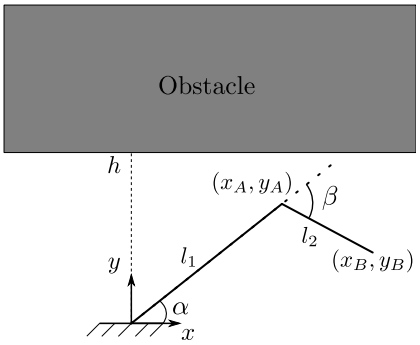

Figure 6: The 2R robot with an obstacle.

To do so, a box atlas of the configuration space for this robot (a torus), is used. The subdivision method SIVIA, presented in [18] and reminded in Section 2.2, is applied on each chart to find all the configurations for which the robot does not collide with the obstacle.

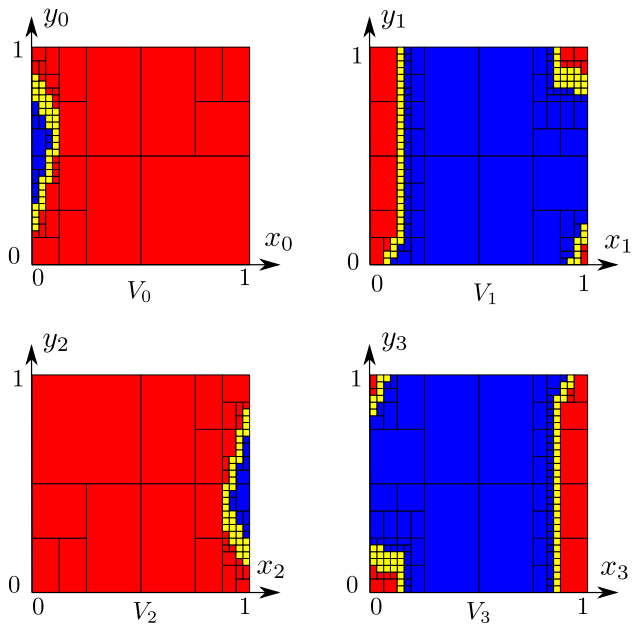

Figure 7: SIVIA algorithm applied to the four charts of the torus box atlas.

The result of the SIVIA algorithm on the four charts is presented on Figure 7 and a representation of SIVIA on the torus is depicted in Figure 8. This representation can be done using the φ_i^{-1} functions. Each box depicted

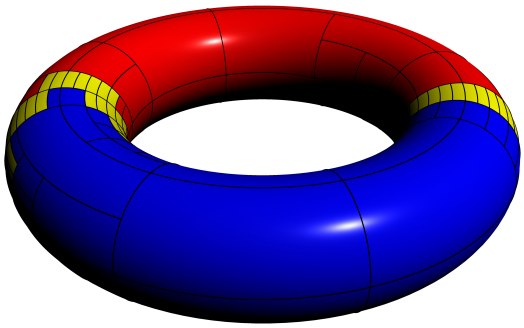

Figure 8: Representation of the result of SIVIA on the torus.

in red represents a set of solutions, thus the set of red boxes represents $\mathbb{X}^-$. The yellow boxes represent configurations for which it is not determined if they are solution or not because the precision ε has been reached. The set of all red and yellow boxes represents $\mathbb{X}^+$. The blue boxes represent the configuration for which the robot intersects the obstacle, they are guaranteed not to be solution.

3.3. Case of the manifold of dimension 2: surfaces

This section presents the construction of a paving which respects the constraints of Definition 2 for every compact manifold of dimension 2 (surfaces). These pavings are made such that a box atlas can be built for each of them.

Theorem 1 is one of the main topology theorems [20, 21]. It gives a classification of all compact manifolds of dimension 2. The operator # represents the connected sum of two surfaces.

Theorem 1. Any compact surface is homeomorphic to the sphere S^2, a handle-body surface $H_g = \overbrace{T^2 \# T^2 \# \ldots \# T^2}^{g \text{ copies}}$ with $g \geq 1$, or a cross-cap surface $C_g = \overbrace{\mathbb{P}^2 \# \mathbb{P}^2 \# \ldots \# \mathbb{P}^2}^{g \text{ copies}}$ with $g \geq 1$.

This theorem makes it possible to represent every surface as a sphere S^2, a connected sum of toruses T^2 or a connected sum of projective planes $\mathbb{P}^2$. Based on this classification, the proposed approach allows to make a paving of every surface. The following subsections present a paving of S^2, a paving of T^2 and a paving of $\mathbb{P}^2$ for which a box atlas can be done and propose a method to build the paving for every surface.

3.3.1. Sphere S^2

The first surface considered is the sphere. Figure 9 represents the fundamental polygon [14] of S^2 with a paving of two charts. Since the two edges are equivalent, they can not be in the same subset U_i of the manifold (because φ_i must be homeomorphisms). Then, one can make a paving of S^2 with two sets U_0 and U_1 that respect the constraints of Definition 2.

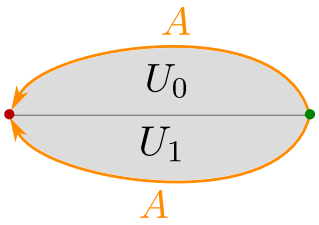

Figure 9: A paving of the sphere with 2 subsets for which a box atlas can be done.

According to the paving $\{U_0, U_1\}$, it is possible to define homeomorphisms in order to build a box atlas of the sphere with two charts.

3.3.2. Handle-body H_g

The second class of surfaces is the handle-body surface H_g. It can be noticed that $H_1 = T^2$ and a paving of T^2 has been presented in section 3.2 with four subsets depicted in Figure 10.

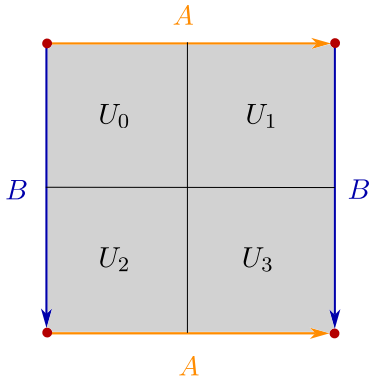

Figure 10: A paving of the torus with 4 charts.

Figure 11 represents the torus with an additional edge **C** that will be used to sum the two torus $T^2 \# T^2$ as depicted in Figure 12.

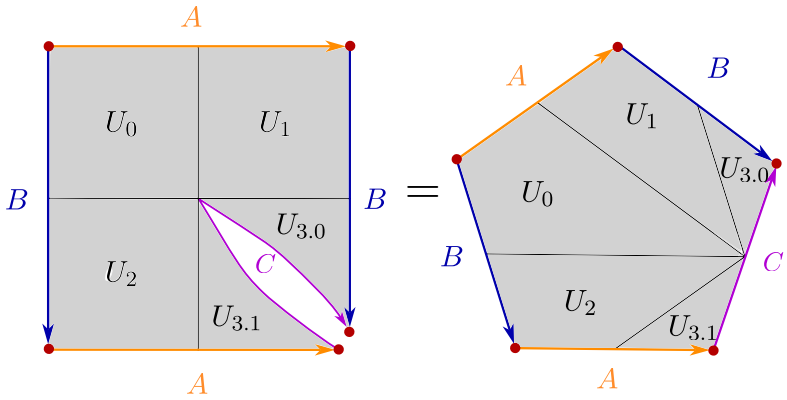

Figure 11: A paving of T^2 with additional edge.

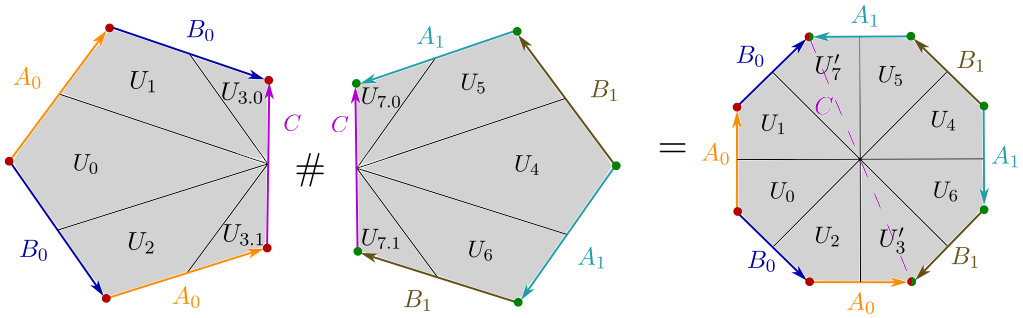

Figure 12: A paving of H_2 with eight subsets for which a box atlas can be done.

Figure 12 presents the construction of the paving of $H_2 = T^2 \# T^2$ according to the paving of T^2. As the paving of H_2 respects the constraints of the Definition 2, a box atlas of H_2 can be obtained with 8 charts (corresponding to the paving of 8 sets $\{U_0 \dots U_7\}$). This construction can be generalized to H_g $(g > 2)$.

Then, a box atlas of the handle-body of genus g $(g \geq 1)$ can be obtained with $4g$ charts.

3.3.3. Cross-cap C_g

The third class of surfaces is the cross-cap surface C_g. It can be noticed that $C_1 = \mathbb{P}^2$. In order to build the paving of C_g $(g > 1)$, let first introduce a paving of $\mathbb{P}^2$. Then, based on the paving of $\mathbb{P}^2$, a method is presented to build a paving of $C_2 = \mathbb{P}^2 \# \mathbb{P}^2$. This method can be extended for all value of $g > 2$.

A paving of the fundamental polygon of $\mathbb{P}^2$ is depicted in Figure 13 with three subsets. Since each vertex is represented twice, then each pair of vertices must be in different subset to respect constraints of Definition 2.

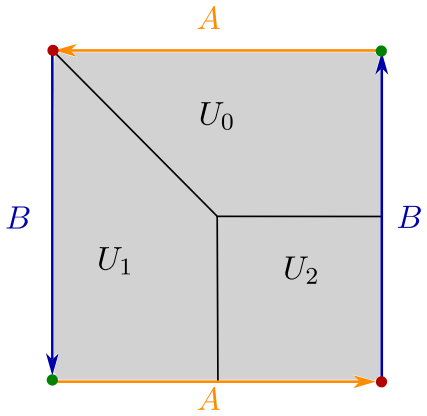

Figure 13: A paving of the projective plane with 3 subsets.

Figure 14 represents the projective plane with an additional edge **C** that will be used to sum the two cross-caps $\mathbb{P}^2\#\mathbb{P}^2$ as depicted in Figure 15.

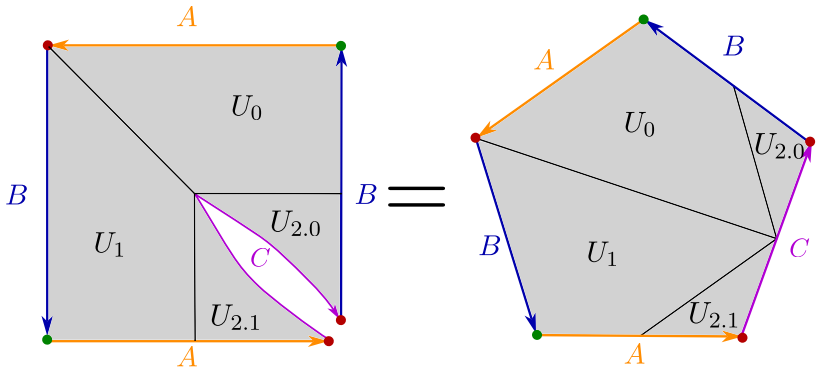

Figure 14: A paving of the projective plane with additional edge.

Figure 15 presents the construction of the paving of $C_2 = \mathbb{P}^2\#\mathbb{P}^2$ according to the paving of $\mathbb{P}^2$. As the paving of C_2 respects the constraints of the Definition 2, a box atlas of C_2 can be obtained with 6 charts (corresponding to the paving of 6 sets $\{U_0 \ldots U_5\}$). This construction can be generalized to C_g $(g > 2)$. Then, a cross-cap of genus g can be described by a box atlas with $3g$ charts.

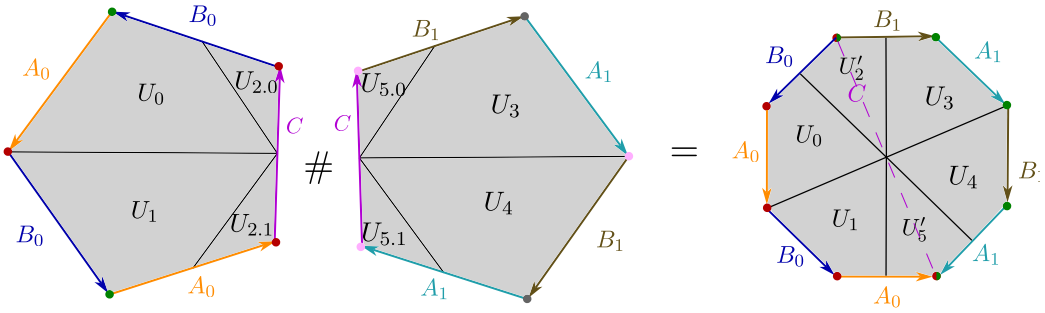

Figure 15: A box atlas of C_2 with six subsets for which a box atlas can be done.

As a conclusion, this section has proposed an iterative construction the box atlas of each class of surfaces. Moreover, the following proposition gives an upper bound of the number of charts needed as a function of the genus of the surface.

Proposition 2. Any orientable surface of genus $g > 0$ admit a box atlas of at most $4g$ charts.

Any non-orientable surface of genus g admit a box atlas of at most $3g$ charts.

Remark. The proposed number of charts for each class of surface may not be the minimal number of charts.

4. Path planning application

This section presents the resolution of a path planning problem using interval analysis and box atlas.

Let's consider a segment AB of length l moving on a quotient space $P_\sim$. $P_\sim$ is the space $P = [0, 2] \times [0, 2]$ quotiented by the relation $\sim$ defined by :

$$(x, y) \sim (x - 2, y) \sim (x, y - 2) \tag{3}$$

Chapter 1, paragraph 7 of [14] explains that such a quotient space is homeomorphic to a torus. $P_\sim$ and segment AB are depicted in Figure 16. The segment AB has three degrees of freedom: the position of the point A $(x_A, y_A) \in P_\sim$ and its orientation $\theta \in S^1$. Its configuration space is the compact manifold $M = P_\sim \times S^1$ (M is homeomorphic to $T^3 = S^1 \times S^1 \times S^1$).

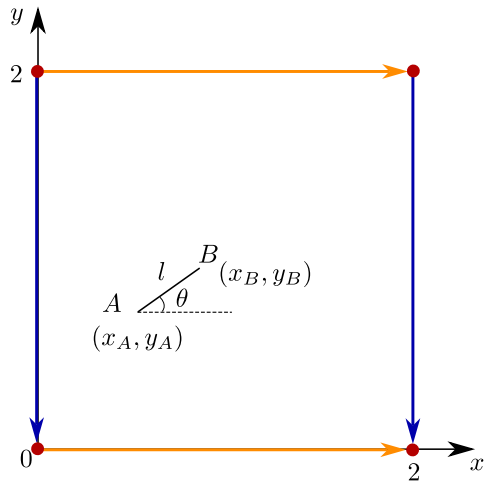

Figure 16: Segment AB on $P_\sim$.

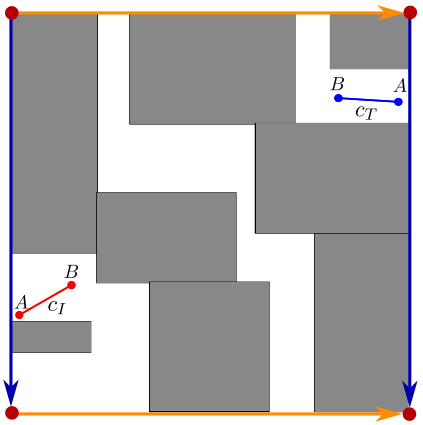

Figure 17: $P_\sim$ with the obstacles.

The goal is to find a guaranteed path for the segment AB, from an initial configuration $c_I = (x_I, y_I, \theta_I)$ to a target configuration $c_T = (x_T, y_T, \theta_T)$, such that the segment AB does not intersect any obstacle as depicted in Figure 17. The resolution of the path planning problem consists in 4 steps: building a box atlas of the configuration space M, compute a subpaving of the allowed configurations in each chart of the box atlas of M using SIVIA, constructing a graph where each box of the subpaving is a node and two boxes are connected if they intersect, finally, applying Dijkstra algorithm [22] to find a path in the allowed configurations from the box that contains c_I to the box that contains c_T. More precisely, the 4 steps are described in the following.

Firstly, a box atlas of the configuration space M is given with eight charts corresponding to eight subsets:

$U_0 = [0,1] \times [0,1] \times [0,\pi]$, $U_1 = [1,2] \times [0,1] \times [0,\pi]$

$U_2 = [0,1] \times [1,2] \times [0,\pi]$, $U_3 = [1,2] \times [1,2] \times [0,\pi]$

$U_4 = [0,1] \times [0,1] \times [\pi,2\pi]$, $U_5 = [1,2] \times [0,1] \times [\pi,2\pi]$

$U_6 = [0,1] \times [1,2] \times [\pi,2\pi]$, $U_7 = [1,2] \times [1,2] \times [\pi,2\pi]$

The eight charts V_i are defined by: $V_i = [0,1] \times [0,1] \times [0,1]$, for $i \in \{0,\ldots,7\}$.

The homeomorphisms φ_i are described in Table 3.

A representation of the box atlas of M with eight charts is depicted in Figure 18. Transition maps τ_{ij} between chart i and chart j can be defined using Equation (1).

φ_0: $\begin{array}{ccc} U_0 & \to & V_0 \\ (x,y,\theta) & \mapsto & (x,y,\theta/\pi) \end{array}$ φ_0^{-1}: $\begin{array}{ccc} V_0 & \to & U_0 \\ (x_0,y_0,z_0) & \mapsto & (x_0,y_0,z_0\cdot\pi) \end{array}$	φ_1: $\begin{array}{ccc} U_1 & \to & V_1 \\ (x,y,\theta) & \mapsto & (x-1,y,\theta/\pi) \end{array}$ φ_1^{-1}: $\begin{array}{ccc} V_1 & \to & U_1 \\ (x_1,y_1,z_1) & \mapsto & (x_1+1,y_1,z_1\cdot\pi) \end{array}$
φ_2: $\begin{array}{ccc} U_2 & \to & V_2 \\ (x,y,\theta) & \mapsto & (x,y-1,\theta/\pi) \end{array}$ φ_2^{-1}: $\begin{array}{ccc} V_2 & \to & U_2 \\ (x_2,y_2,z_2) & \mapsto & (x_2,y_2+1,z_2\cdot\pi) \end{array}$	φ_3: $\begin{array}{ccc} U_3 & \to & V_3 \\ (x,y,\theta) & \mapsto & (x-1,y-1,\theta/\pi) \end{array}$ φ_3^{-1}: $\begin{array}{ccc} V_3 & \to & U_3 \\ (x_3,y_3,z_3) & \mapsto & (x_3+1,y_3+1,z_3\cdot\pi) \end{array}$
φ_4: $\begin{array}{ccc} U_4 & \to & V_4 \\ (x,y,\theta) & \mapsto & (x,y,(\theta-\pi)/\pi) \end{array}$ φ_4^{-1}: $\begin{array}{ccc} V_4 & \to & U_4 \\ (x_4,y_4,z_4) & \mapsto & (x_4,y_4,(z_4+1)\cdot\pi) \end{array}$	φ_5: $\begin{array}{ccc} U_5 & \to & V_5 \\ (x,y,\theta) & \mapsto & (x-1,y,(\theta-\pi)/\pi) \end{array}$ φ_5^{-1}: $\begin{array}{ccc} V_5 & \to & U_5 \\ (x_5,y_5,z_5) & \mapsto & (x_5+1,y_5,(z_5+1)\cdot\pi) \end{array}$
φ_6: $\begin{array}{ccc} U_6 & \to & V_6 \\ (x,y,\theta) & \mapsto & (x,y-1,(\theta-\pi)/\pi) \end{array}$ φ_6^{-1}: $\begin{array}{ccc} V_6 & \to & U_6 \\ (x_6,y_6,z_6) & \mapsto & (x_6,y_6+1,(z_6+1)\cdot\pi) \end{array}$	φ_7: $\begin{array}{ccc} U_7 & \to & V_7 \\ (x,y,\theta) & \mapsto & (x-1,y-1,(\theta-\pi)/\pi) \end{array}$ φ_7^{-1}: $\begin{array}{ccc} V_7 & \to & U_7 \\ (x_7,y_7,z_7) & \mapsto & (x_7+1,y_7+1,(z_7+1)\cdot\pi) \end{array}$

Table 3: Homeomorphisms for the box atlas of $P_\sim$.

Secondly, the algorithm SIVIA is used in each chart to compute an approximation of the allowed configurations set using homeomorphisms φ_i and a collision test. It gives eight subpavings $\mathbb{X}_i^-$ of the guaranteed allowed configuration for each chart. Let denote by $\mathbb{X}^- = \bigcup_{i\in I} \mathbb{X}_i^-$ the set of allowed configurations.

Thirdly, the Algorithm 1 is used to build the graph $\mathcal{G}$. The set of nodes of $\mathcal{G}$ corresponds to each boxes of the subpaving of $\mathbb{X}^-$. Two boxes are connected in $\mathcal{G}$ if their intersection is not empty. Note that because two boxes in different charts may intersect, the intersection between two boxes is computed using the transition maps τ_{ij} line 8 of Algorithm 1. The weight

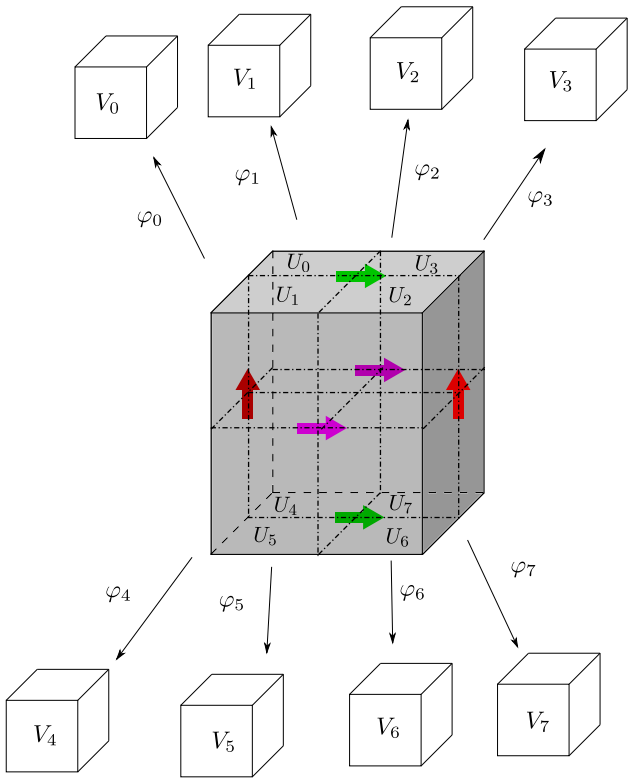

Figure 18: The eight charts box atlas of $M = T^3$.

of the edges are set to 1 to compute the minimum number of boxes line 8. This weight is chosen arbitrarily, [23] proposes other methods to compute the weight of the edges.

Algorithm 1 Construction of the graph $\mathcal{G}$

Require: a list of boxes $\mathcal{L}$ subpaving of $\mathbb{X}^-$, the box atlas

Initialization: The nodes of $\mathcal{G}$ are the boxes of $\mathcal{L}$
while $\mathcal{L}$ not empty **do**
    $\mathbf{x}_0 = \text{pop}(\mathcal{L})$
    for all $\mathbf{x}_1$ in $\mathcal{L}$ **do**
        i is number of the chart of $\mathbf{x}_0$
        j is number the chart of $\mathbf{x}_1$
        if $\mathbf{x}_0 \cap \tau_{ji}(\mathbf{x}_1) \neq \emptyset$ **then**
            Create the edge between $\mathbf{x}_0$ and $\mathbf{x}_1$
            Set the weight of the edge to 1
        end if
    end for
end while
return $\mathcal{G}$

Finally, the algorithm Dijkstra is applied on $\mathcal{G}$ to find a path from c_I to c_T, in the allowed configuration space.

The result of this approach for the path planning problem is presented in Figure 19. In the representation of the eight charts, the red boxes are the boxes that are in the solution path, the solid black lines are the connections between two boxes in the same chart and the dotted blue lines are the connections between two boxes that are in different charts.

Figure 20 shows the path obtained (the drawn positions correspond to the center of each red box).

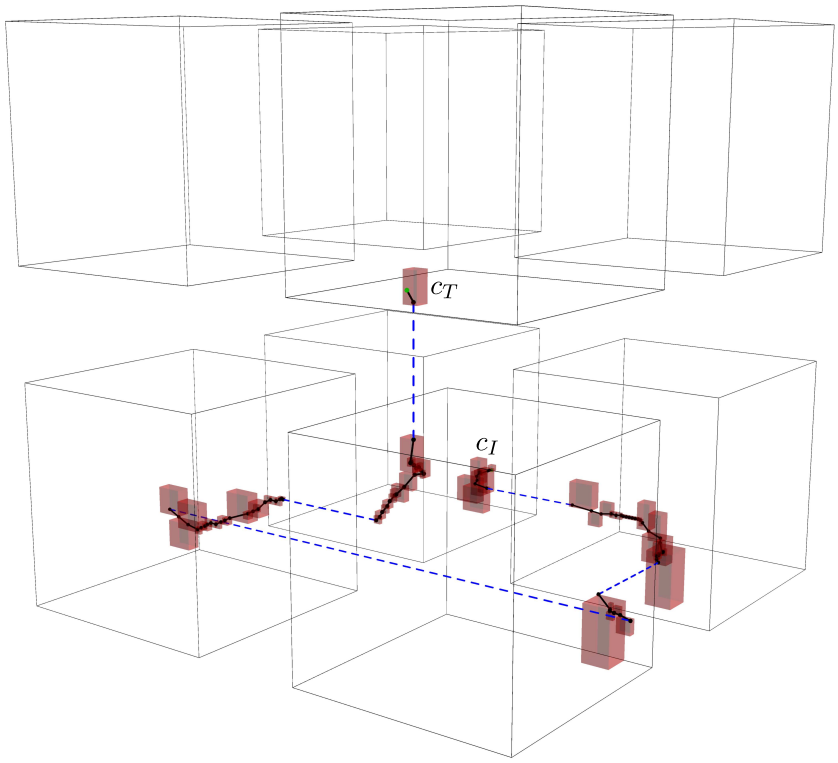

Figure 19: Result of Dijkstra.

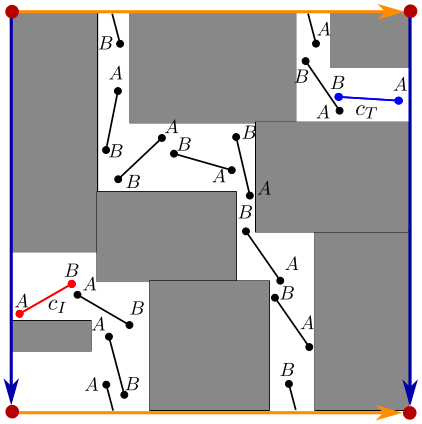

Figure 20: Representation of the steps of Dijkstra.

5. Conclusion

In this paper, the notion of box atlas is introduced and illustrated, with emphasis on its benefits. It has been detailed how to build a possible box atlas from a compact manifold. The box atlas makes it possible to link the notions of atlas, and then manifolds, to interval analysis. This offers the possibility of using interval analysis tools on not primary boxable spaces, for example configuration spaces of robots. Two important notions of robotics and mathematics are now joined: manifolds and interval analysis, permitting to have guaranteed solutions on a large class of manifold related problems.

Box atlas can be seen as an alternative of "bisectable abstract domains" and allow applying interval analysis based method on manifold where a lattice structure not exist.

Future work will focus on use box atlas to the resolution of path planning robotic problems in 3 dimensional manifolds like $SO(3)$ or $\mathbb{P}^3$. Also, the box atlas seems to be "extendable" to the manifolds with boundaries such as the closed disk or the Möbius band. Finally, a perspective is also to find a general procedure to obtain a box atlas of compact manifolds.

References

[1] Eric O Korman. Self-supervised representation learning on manifolds. In ICLR 2021 Workshop on Geometrical and Topological Representation Learning, 2021.

[2] R.E. Moore. Interval Analysis. Prentice-Hall series in automatic computation. Prentice-Hall, 1966.

[3] Luc Jaulin, Michel Kieffer, Olivier Didrit, and Eric Walter. Applied Interval Analysis with Examples in Parameter and State Estimation, Robust Contro Springer London Ltd, August 2001. https://link.springer.com/book/10.1007/978-1-4471-0249-6.

[4] A. Piazzi and A. Visioli. Global minimum-jerk trajectory planning of robot manipulators. IEEE Transactions on Industrial Electronics, 47(1):140–149, 2000.

[5] Michel Kieffer, Luc Jaulin, Éric Walter, and Dominique Meizel. Robust autonomous robot localization using interval analysis. Reliable computing, 6(3):337–362, 2000.

[6] Rémy Guyonneau, Sébastien Lagrange, Laurent Hardouin, and Philippe Lucidarme. Guaranteed interval analysis localization for mobile robots. Advanced Robotics, 28(16):1067–1077, July 2014.

[7] L. Jaulin. Interval analysis and robotics. In SCAN'12, Novosibirsk, Russia, 2012.

[8] Jean B. Lasserre. Global optimization with polynomials and the problem of moments. SIAM Journal on Optimization, 11(3):796–817, 2001.

[9] L. Jaulin, B. Desrochers, and D. Massé. Bisectable Abstract Domains for the resolution of equations involving complex numbers. Reliable Computing, 23:35–46, 2016.

[10] Michael Watterson, Sikang Liu, Ke Sun, Trey Smith, and Vijay Kumar. Trajectory optimization on manifolds with applications to quadrotor systems. The International Journal of Robotics Research, 39(2-3):303–320, 2020.

[11] Ahmed H. Qureshi, Jiangeng Dong, Austin Choe, and Michael C. Yip. Neural manipulation planning on constraint manifolds. IEEE Robotics and Automation Letters, 5(4):6089–6096, 2020.

[12] NARONGDECH KEERATIPRANON, FREDERIC MAIRE, and HENRY HUANG. Manifold learning for robot navigation. International Journal of Neural Systems, 16(05):383–392, 2006. PMID: 17117499.

[13] Edward Y. L. Gu. A configuration manifold embedding model for dynamic control of redundant robots. The International Journal of Robotics Research, 19(3):289–304, 2000.

[14] Loring W. Tu. An Introduction to Manifolds. Universitext. Springer New York, New York, NY, 2011.

[15] Sylvain Calinon. Gaussians on riemannian manifolds: Applications for robot learning and adaptive control. IEEE Robotics & Automation Magazine, 27(2):33–45, 2020.

[16] Marina Meilă and Hanyu Zhang. Manifold learning: What, how, and why. Annual Review of Statistics and Its Application, 11(Volume 11, 2024):393–417, 2024.

[17] José Luis Blanco-Claraco. A tutorial on **SE**(3) transformation parameterizations and on-manifold optimization, 2022.

[18] L. Jaulin and E. Walter. Set inversion via interval analysis for nonlinear bounded-error estimation. Automatica, 29(4):1053–1064, 1993.

[19] V. Lumelsky. Effect of kinematics on motion planning for planar robot arms moving amidst unknown obstacles. IEEE Journal on Robotics and Automation, 3(3):207–223, 1987.

[20] M.P. Hitchman. Geometry with an Introduction to Cosmic Topology. Geometry with an Introduction to Cosmic Topology. Jones and Bartlett Publishers, 2009.

[21] GeorgeK. Francis and JeffreyR. Week. Conway'szip proof. American Mathematical Monthly, 106(5):393–399, 1999.

[22] Huijuan Wang, Yuan Yu, and Quanbo Yuan. Application of dijkstra algorithm in robot path-planning. In 2011 Second International Conference on Mechanic Automation and Control Engineering, pages 1067–1069, 2011.

[23] L. Jaulin. Path planning using intervals and graphs. Reliable Computing, 7(1):1–15, 2001.